Investigation into Boundary Layer Transition on the MEXICO Blade

IOP Conf. Series: Journal of Physics: Conf. Series **1037** (2018) 052020 doi:10.1088/1742-6596/1037/5/052020

Investigation into Boundary Layer Transition on the MEXICO Blade

B A Lobo[1], K Boorsma[2] and A P Schaffarczyk[3]

[1] Wind Energy Technology Institute, University of Applied Sciences Flensburg, Germany
[2] ECN, Westerduinweg 3, 1755 LE Petten, The Netherlands
[3] Department of Mechanical Engineering, University of Applied Sciences, Kiel, Germany

E-mail: brandon.lobo@stud.fh-flensburg.de

Abstract. Boundary layer transition studies have been carried out using the unsteady surface pressure data from the EU project MEXICO and the later New-MEXICO experiment at the DNW wind tunnel, which have been subject of investigation in IEA Wind Task 29 Mexnext. The experiments were conducted on a specially designed 4.5 m diameter wind turbine with and without zig-zag roughness strips applied to the outboard part of the blades. Standstill tests with the MEXICO blades were also conducted at the TU Delft LTT wind tunnel including oil flow and stethoscope tests.

Transition is determined by detecting and observing the growth of Tollmien-Schlichting (TS) packets through a Power Spectral Density plot in the frequency domain. The expected frequency range of these waves is determined using a database developed by Van Ingen. The transition results are compared to those determined by RFOIL, a program for the analysis of aerofoils which uses the e^N method for transition detection. Generally a good agreement was observed between measurements and predictions. In addition to that the effectiveness of the roughness strips was studied. The result is a unique database in controlled conditions to be used for validation and improvement of transition modelling of wind turbine blades.

1. Introduction

The transition from a laminar to a turbulent boundary layer has a profound influence on the performance of an airfoil. Factors such as the lift and drag force are influenced by the type of flow within the boundary layer [1]. Optimal airfoil design aims at achieving a predetermined level of performance by balancing these conditions with the knowledge of the transition point at specified inflow conditions. To successfully accomplish this and develop an airfoil with the desired flow characteristics, it is necessary to have access to validated aerodynamic models whose results can be verified through experiments under controlled conditions.

With this intention, boundary layer transition studies were carried out on the data collected from the EU project MEXICO [2] and the following New-MEXICO experiment [3] which have been subject of investigation in IEA Wind Task 29 Mexnext [4] [5]. These measurements were carried out on a model specifically designed for the purpose, with a rotor diameter of 4.5 m, placed in the largest European wind tunnel: the LLF facility of the German-Dutch Wind Tunnel, DNW. Another experimental study on the blade of this rotor was carried out at TU Delft's LTT wind tunnel [3]. In addition to these experiments, oil flow tests and stethoscope tests were also carried out at the TU Delft LTT wind tunnel to determine the location of laminar to turbulent transition.

2. Objectives

The following objectives were identified for this project:

- Determination of a method to locate the transition region and a possible frequency range of the corresponding Tollmien-Schlichting disturbances which eventually lead to transition.
- Verification whether laminar to turbulent transition could be detected for the flow conditions under which the experiments were conducted using pressure sensors with a data acquisition frequency of 5.5 kHz .
- Analysis of the data collected from the MEXICO, New-MEXICO and TU Delft LTT wind tunnel experiments to determine a laminar to turbulent transition detection algorithm and a corresponding script to automate the process.
- Computation and comparison of the detected transition to RFOIL, the stethoscope tests and the oil flow tests on the outer-board part of the blade (82%R and 92%R, with R indicating span) which corresponds to the NACA64-418 profile only.

3. Test Set-Up

Figure 1 illustrates the test set-up of the experiments. The MEXICO model features a three-bladed 4.5m diameter upwind rotor, including a speed controller and pitch actuator. The model is instrumented with flush mounted unsteady pressure sensors at five sections (25%R,35%R, 60%R, 82%R, and 92%R), distributed over the three blades. All sections were equipped with 25-28 sensors, each with a sample rate of 5.5 kHz.

(a) New-MEXICO test set-up (b) Delft LTT set-up

Figure 1: Illustrations of the experimental set-up

The New-MEXICO experiment consisted of tests with and without a zig-zag roughness strip in both, standstill and rotating conditions. The MEXICO experiment, however, only included tests with the roughness strip in place. The experiment on the MEXICO blade at standstill at TU Delft included tests without a roughness strip as well as tests with roughness strips of different dimensions as specified in table 1. Stethoscope and oil-flow tests were also carried out here.

For the tests with the roughness strip, they were applied on both the pressure and suction side with an identical configuration on each blade. Figure 2(a) shows an illustration of the roughness strip on the pressure side. The strip configuration and location was chosen to minimise unwanted disturbances apart from the desired laminar to turbulent transition. To prevent the zigzag strips from blocking the pressure sensors and/or measuring local pressure disturbances due to the strip, they were interrupted at the location of the sensors on both the pressure and suction side leaving

Table 1: Zig-Zag strip dimensions

		Thickness [mm]	Width [mm]
DNW wind tunnel experiments		0.200	10
TU Delft wind tunnel experiment	StripA	0.185	5
	StripB	0.110	5

† The oil-flow tests used only StripA.

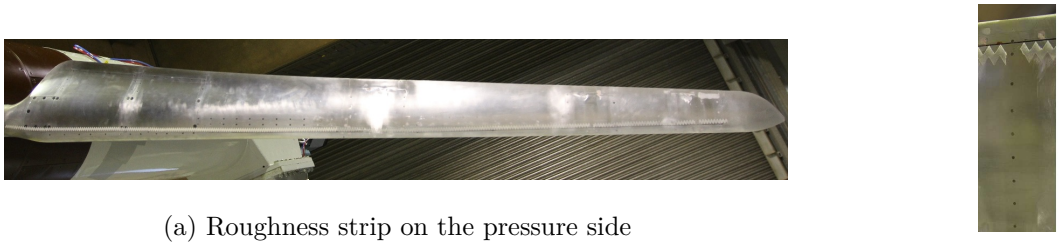

(a) Roughness strip on the pressure side

(b) Strip interruption at 60%R

Figure 2: New-MEXICO zig-zag roughness strip [6]

a gap of approximately 10 mm (5 mm on both sides of the sensor) [6]. Figure 2(b) shows the interrupted strip. It was anticipated that span-wise wedges arising from the strip edges would trip the boundary layer even at the location of the pressure sensors, albeit slightly downstream. Note that the strip on the suction side of the blade, for the TU Delft Wind Tunnel experiments was uninterrupted, as pointed out in table 2. It was however, taped over when the pressure sensors were covered during the oil-flow test as seen in figure 3. Table 2 shows the chord-wise location of the roughness strip on the New-MEXICO experiment at 82%R and 92%R. This corresponds to the NACA64-418 sections that were analysed as a part of this project.

Table 2: Zig-Zag strip configuraton [7]

Roughness strip: New-MEXICO experiment			Was the roughness strip interrupted in the vicinity of the sensors? See: figure 2(b)	
Location	82% span	92% span	DNW Wind Tunnel	TU Delft Wind Tunnel
Pressure Side	17%	19%	Yes	Yes
Suction Side	17%	19%	Yes	No

4. Methodology

The amplification of initial disturbances, the Tollmien-Schlichting (T-S) waves are the first indicator of laminar flow instability [8]. To locate transition from the data collected, it is necessary to locate the T-S waves by determining the frequency range where they occur. This is possible from stability plots which are generated on solving the Orr-Sommerfeld equation for its Eigen solutions, independently, and at every chord position. This is, even today, a computationally involved process and it is not unusual for airfoil design computations to use a database of pre-computed results for a series of boundary layer velocity profiles. The Hartree and Stewartson solutions of the Falkner-Skan equation are generally used [9].

Stability analysis can be carried out either in spatial or temporal mode. Arnal [10] carried out a spatial mode stability analysis for 15 Hartree/Stewartson solutions of the Falkner-Skan equation. Using these results, Van Ingen has developed a database method which generates

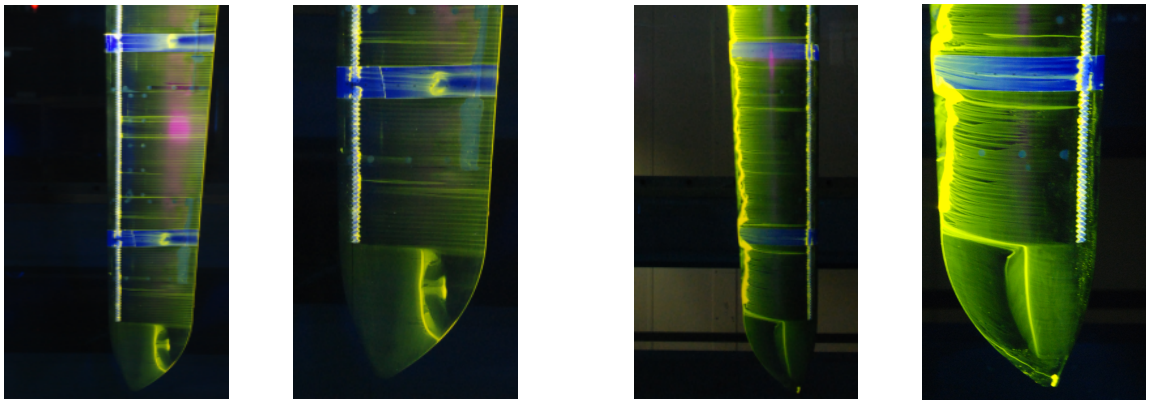

(a) Pressure side: Strip is interrupted (b) Suction side: Strip is uninterrupted

Figure 3: TU Delft wind tunnel oil flow test, AOA: 5°. Laminar flow is seen as a relatively dark region. Bright regions indicate that the oil is not being transported across the surface.

stability diagrams for different Hartree velocity profiles [11] based on the boundary layer velocity shape factor and the flow Reynolds number. This database and the corresponding matlab files are published on a CD-ROM [12] and were available for use. Since stability plots are calculated at every chord location, each location could be analysed as a different Hartree profile [9].

As stated by Van Ingen [9], the main factors determining stability can be reduced to the shape of the boundary layer velocity profile, the momentum loss Reynolds number and the frequency of the initial disturbances within the boundary layer. To predict the frequency range where the growth of the T-S disturbances takes place for the MEXICO blade under the conditions of the experiment, it is necessary to know the boundary layer shape factor and the critical momentum loss Reynolds number for each case.

4.1. Expected Frequency Range of Tollmien-Schlichting Waves from a Given Database
Firstly, from the measured tunnel speed, rotational speed and pitch angle, local angles of attack (AOA) are estimated using a BEM tool, together with the Reynolds number. Then, RFOIL [13] for the corresponding amplification factor [7] was used to determine the shape factor along the chord. Van Ingen's database method was used to determine the critical momentum loss Reynolds number as it agrees well with the critical momentum loss Reynolds number calculated by Arnal [9].

Van Ingen's database together with the output from RFOIL was utilised to determine the expected frequency range of the T-S waves. The matlab files from the CD-ROM [12] work with the database by iterating through a range of initial disturbance amplitudes over a defined frequency range to internally generate stability plots at every defined chord location beyond the instability point. At every chord location, for a given frequency, the disturbance could increase in amplitude, be damped down or have no change. The markers seen in figure 4(a) and 4(b) represent an increase in amplitude, the absence of which indicates no change or a damping at that particular frequency. For every frequency considered at a specific chord location, the disturbance grows by a factor N. Where N is the ratio of the amplitude of the disturbance at the chord position being considered to the initial amplitude. The maximum of the different amplification values at different frequencies at a particular chord location is Nmax [12].

From figure 4(a) it is expected to see an increase in energy up to a frequency of around 1200 Hz at 60% chord (experimental sensor location) on the pressure side. On the suction side as seen in figure 4(b), at 62.86% chord (experimental sensor location) an increase in energy up to a frequency of around 1700 Hz could be expected.

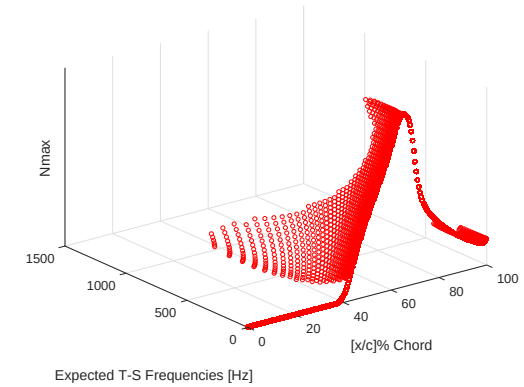

(a) Pressure side expected frequencies (computations)

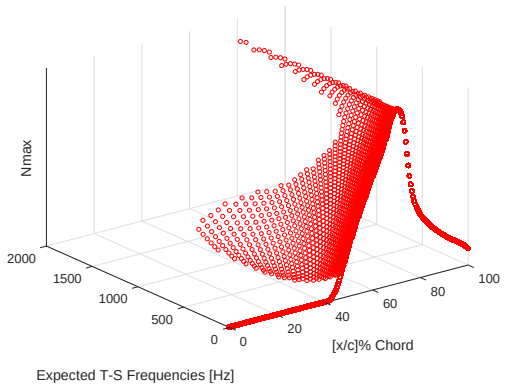

(b) Suction side expected frequencies (computations)

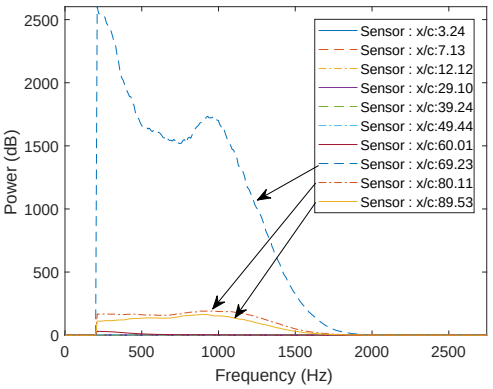

(c) Observed frequencies (PSD plots, pressure side)

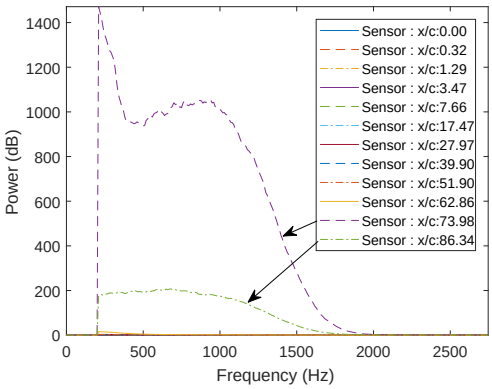

(d) Observed frequencies (PSD plots, suction side)

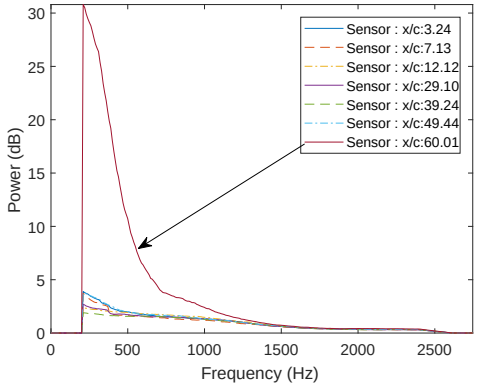

(e) Pressure side PSD plot zoomed in (from the figure above) to view T-S disturbance at 60% chord

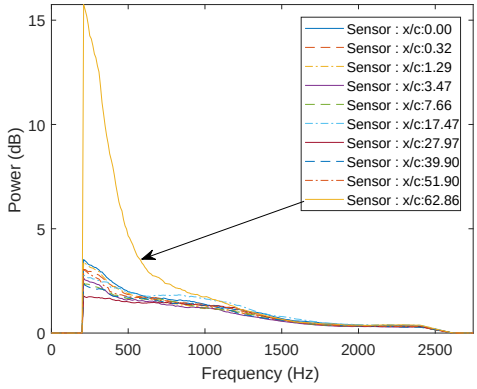

(f) Suction side PSD plot zoomed in (from the figure above) to view T-S disturbance at 62.86% chord

Figure 4: Expected and observed frequencies (without roughness strip) for the New-MEXICO experiment at standstill, 92% blade span, Re: 2.39×10^5, AOA: -1.3°

4.2. Data Processing

The experimental time-series data must be converted into the frequency domain before analysing the power spectral density (PSD) plots to determine if a similar frequency range, as predicted sees an increase in energy. Ideally, a slice of figures 4(a) and 4(b) at a particular chord location in a plane parallel to the axis Nmax and perpendicular to the chord axis should be expected to

be seen on the PSD plot of the run under the same inflow conditions.

Each of the Kulite® pressure sensors had a sampling rate of 5514 Hz and each run was carried out for a little over five seconds resulting in 27610 readings at each sensor. The data collected is first calibrated and made fit for work. Details are found in [7] and [14].

Next, the low frequency disturbances which are caused due to the RPM of the rotor, the electrical noise, etc. were removed, by filtering out frequencies of 200 Hz and lower. This range was chosen, as it was here where noise was seen in the frequency domain. Also, the T-S disturbances are expected up to 1500 or 2000 Hz depending on the run conditions, so filtering out the low frequency components should not hamper the results. Using a Fourier transform, the time-series data was transformed to the frequency domain and a band pass filter which retained frequencies above 200 Hz up to 2757 (5514/2 Hz) Hz, the Nyquist frequency was applied. Then, an inverse Fourier Transform was used to obtain a new time-series signal [7].

The filtered time-series data was then divided into blocks, following which the PSD of each block was separately calculated. The PSD of these blocks was averaged by summing up the values (dB) in each frequency band across every block before averaging the vector. This results in a single PSD at a given chord position for the run in consideration. No critical data was lost by averaging the PSD plots this way, as the end goal is the observation of a trend and increases in energy within specific frequency ranges.

Visually being able to observe increases in energy is a critical step in writing an algorithm to detect transition. Therefore, it was decided to work with 50 blocks for this project. A further increase in the number of blocks did not result in visual improvements of the PSD.

The averaged PSD plots did have some peaks at certain frequencies. Similar peaks were seen across multiple sensors under different inflow conditions [7]. This pointed to the fact that they were caused by a phenomenon other than transition. A moving line average was used to smooth out these peaks by considering 10 data points before and 10 points after the point being smoothed out. From stability theory it is clear that Tollmien-Schlichting waves increase in amplitude over a frequency range and not at a single frequency band, so the smoothing of these peaks should not affect the overall results.

Figure 4(c) and 4(d) show the PSD at 92%R for the run at which the expected T-S disturbance frequencies were determined. On the pressure side at 60% chord T-S disturbances are seen with an increase in energy up to approximately 1200 Hz, the same range as predicted. On the suction side, an increase up to 1000 Hz is seen at 62.86% chord, this doesn't exactly agree with the expected 1700 Hz, but it shows that the T-S waves can be detected from the PSD plots and that they are in this general frequency range for which data has been collected. Transition can be visualised at 69.23%R on the pressure side and 73.98%R on the suction side by the increase in energy between 1200 Hz to 1500 Hz when compared to upstream sensors. This is in agreement with the algorithm developed (described in the following section) and also RFOIL which predicts transition at 61.57%R and 67.15%R respectively.

4.3. Transition Detection Algorithm

The algorithm to detect transition depended on the test type: whether it was in standstill or rotating condition and in part on the experiment being analysed on account of the Reynolds number. A single algorithm could not be used for all runs because of a difference in energy levels on the PSD plot. The algorithm was developed on observing the PSD plots in the region of expected T-S disturbances [7].

After data processing it was realised that the initial form of the algorithm produced erroneous results if leading edge separation occurs. As discussed in [7], leading edge separation occurred in some runs at higher angles of attack as evident from pressure distribution plots. The sensor at 0% chord had observable differences in energy at the 200 to 300 Hz frequency range in cases of leading edge separation when compared to the other runs. For the standstill cases an energy

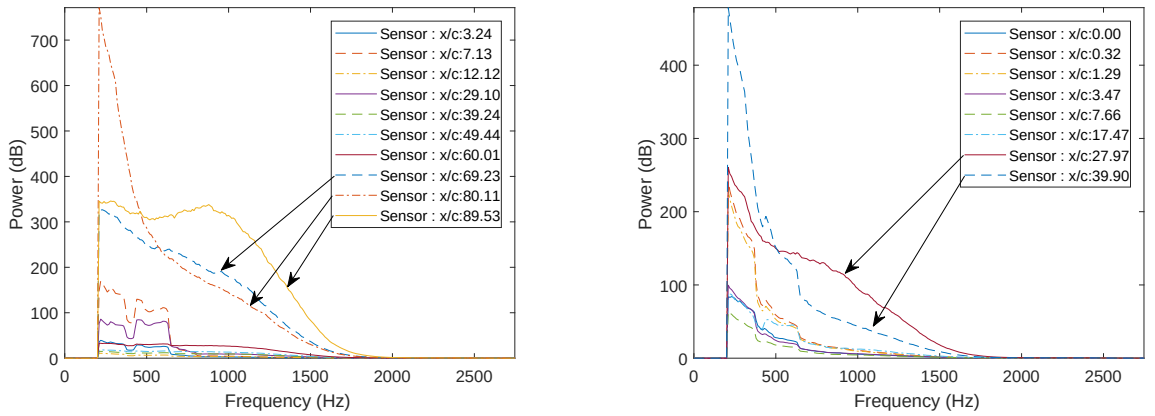

(a) Pressure side: Transition at 69.23% chord (b) Suction side: Transition at 27.97% chord

Figure 5: New-MEXICO 425 RPM 92% span, AOA: 7°, Re: 7.47 X 10^5 with the roughness strip

above 20 dB at 0% chord indicated leading edge separation (500 dB for the rotating runs). The runs without leading edge separation had far lower energies at this chord location, for instance, the energy never exceeded 3 dB for the standstill runs.

4.3.1. Standstill Pitch Traverse The pitch traverse test swept a wide range of pitch angles from -2.3° to 90°. The algorithm was set up with the following conditions:

- Separation: Separation was detected if the maximum energy between 200 to 300 Hz at the first sensor at 0% chord exceeded 20 dB.
- Transition Pressure Side: Transition was set to be that chord position where the area under the curve between 1200 to 1500 Hz at a particular sensor and all the sensors downstream of this sensor was greater than five times the area under the first sensor.
- Transition Suction Side: Transition on the suction side was defined at the chord position where the area under the curve between 1200 to 1500 Hz at a particular sensor and all the sensors downstream of this sensor exceeded 50 dB^2.

Transition using this algorithm has already been discussed for standstill at the end of section 4.2 with the help of figures 4(c) and 4(d).

4.3.2. Rotating Runs The rotating runs consisted of tests at 425 RPM and 325 RPM covering a range of tip speed ratios and pitch angles. The algorithm to detect transition was the same for all rotating runs of the New-MEXICO experiment, the conditions were as follows:

- Separation: Leading edge separation was detected if the maximum energy between 200 Hz to 300 Hz at the first sensor at 0% chord exceeded 500 dB.
- Transition pressure side: Transition is detected at that sensor where the area in dB between 1000 Hz to 2000 Hz is greater than 20 times the area at the first sensor.
- Transition suction side: Transition on the suction side is detected at the sensor where the area between 1500 Hz to 2000 Hz is greater than 1.5 times the area at the first sensor near the leading edge.

A rotating run is seen in figure 5. Using the script developed, transition was detected at 69.23% chord on the pressure side and 27.97% chord on the suction side at 92%R. RFOIL predicts transition at 70.24% and 25.49% chord respectively. Thus there is good agreement.

4.4. Verification of the Script

Oil flow images and stethoscope test results form the TU Delft Wind Tunnel were used to verify the working of the transition detection script. Additionally, the results of the runs without the roughness strip were also compared to RFOIL.

For the oil flow test, on the suction side at an AOA of 5°, as seen in figure 3(b), transition occurs immediately downstream of the strip, as characterised by the bright region behind the strip. The script also detects transition on the sensor immediately behind the strip at 17.47% chord as seen in figure 6(a) at a 5° AOA. On the pressure side, see figure 3(a), the strip is interrupted and transition can be seen over the sensors as the bright yellow region around 50% chord at an AOA of 5°. The transition script detects transition at 49.44% chord, see figure 6(c).

For a Reynolds number of 2.7 $\times$ 10^5 and 35 ms^{-1} without the roughness strip, transition was detected at 55% chord at an AOA of -1.8°. Due to the difference in Reynolds number this cannot be directly compared to the detected transition points at 60 ms^{-1} (Re: 4.5 $\times$ 10^5), nonetheless, a good agreement can be seen in figure 6(a). For the stethoscope test with two different roughness strips, there is a very good agreement between the transition script and the stethoscope results, as seen in figure 6(b) with transition being detected on the sensor directly upstream of the point where transition was heard using the stethoscope.

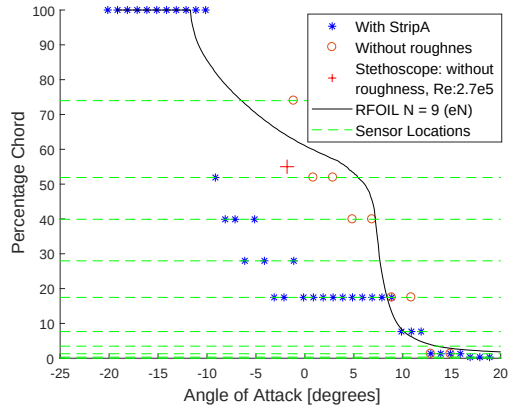

(a) Comparison with and without the roughness strip, suction side, 82% span

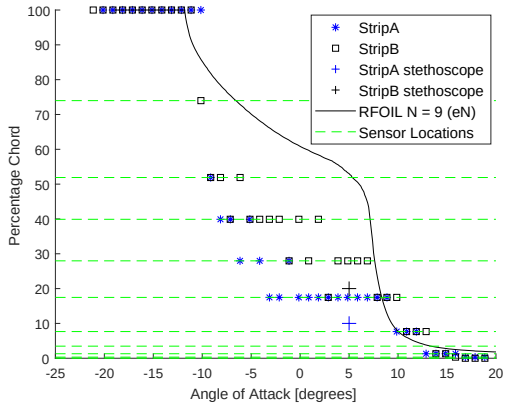

(b) Comparison between different roughness strips, suction side, 82% span

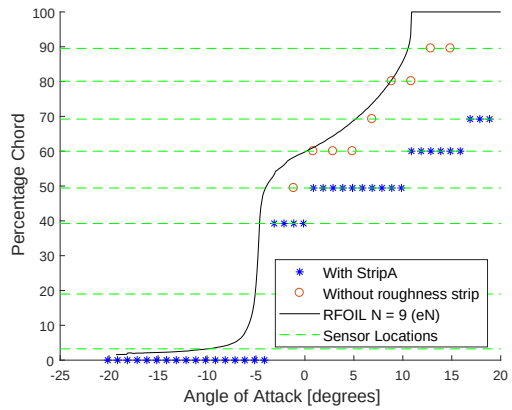

(c) Comparison with and without the roughness strip, pressure side, 82% span

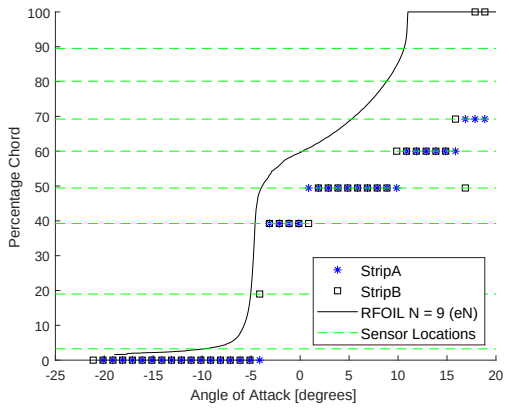

(d) Comparison between different roughness strips, pressure side, 82% span

Figure 6: 2D Blade test LTT, Delft at 82% span, Re: 4.5 $\times$ 10^5

Also, there is a very good agreement between the transition detected for the runs without the roughness strip when compared with RFOIL, as seen in figures 6(a) and 6(c).

5. Results

Using the developed prediction algorithm, transition has been successfully detected for the three experiments and some interesting observations were made.

5.1. Effect of the Roughness Strip

It is clear from the results of figures 6(a), 6(c) and 7 that the roughness strip does cause transition to move upstream. For set-ups where the strip is interrupted, transition is not directly downstream of the strip, but slightly upstream compared to free transition. For the runs without the roughness strip, a good agreement with RFOIL is seen.

It was also observed that the total energy in dB at transition within the observed frequency range (up to 2757 Hz) was higher in case of the runs without the roughness strip on both the pressure and suction side. The higher energy observed in runs with free transition could be due to the free growth of T-S disturbances which is hindered in the presence of a roughness strip as it modifies the boundary layer flow. Further details and plots are found in [7].

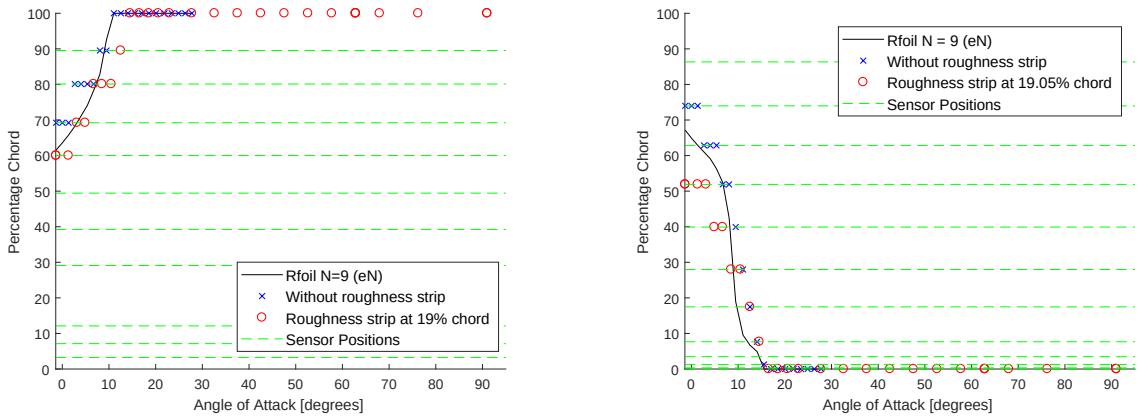

(a) Pressure side (b) Suction side

Figure 7: Effect of roughness strip, New-MEXICO standstill at 92% span, Re: 2.39×10^5

5.2. Reynolds Number Effect

Figure 8 shows the change in transition location based on Reynolds number by comparing the runs with 325 RPM and 425 RPM in the New-MEXICO experiment. As expected, a clear trend with transition occurring further downstream for the lower Reynolds number is seen. More results analyzing the effect of Reynolds number can be found in [7].

An analysis of the data also showed that, the frequency range where T-S waves are observed continue to have elevated energy levels even in turbulent flow. Therefore, a fine distribution of sensors is not necessary to detect the occurrence of transition. However, to know the exact location where it occurs, a fine distribution of sensors is required.

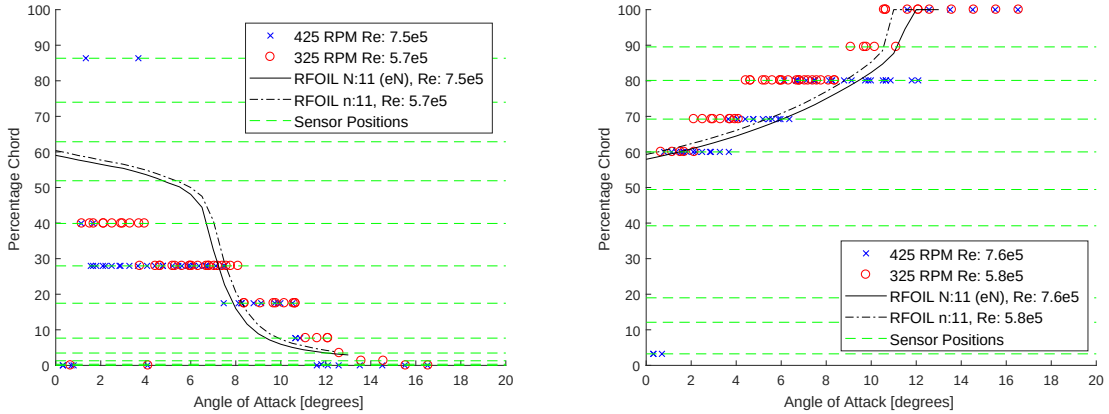

(a) Suction side 92% span (b) Pressure side 82% span

Figure 8: Reynolds number comparison: New-MEXICO rotating without roughness strip

6. Conclusions

Through the work carried out from transient Kulite pressure data, and in accordance with the original goal, the transition location in the MEXICO experiments was successfully determined. The algorithm adopted could easily be extended to other experimental studies.

Generally a good agreement was observed between measured and predicted transition locations. In addition to that, the effectiveness of the roughness strips was successfully studied. The result is a unique database in controlled conditions to be used for validation and improvement of transition modelling of wind turbine blades.

References

[1] Schaffarczyk A P 2014 *Introduction to Wind Turbine Aerodynamics* (Berlin Heidelberg: Springer-Verlag) chapter 3 pp 40 - 5
[2] Schepers J G and Snel H 2007 Model experiments in controlled conditions ECN-E-07-042
[3] Boorsma K and Schepers J G 2014 New MEXICO experiment preliminary overview with initial validation ECN-E–14-048
[4] Schepers J G et al. 2012 Final report of IEA task 29, Mexnext (Phase 1) ECN-E-12-004
[5] Schepers J G et al. 2014 Final report of IEA wind task 29: Mexnext (Phase 2) ECN-E–14-060
[6] Boorsma K, Schepers J G 2018 Description of experimental setup ECN-X–15-093-v3
[7] Lobo B A 2018 Investigation into boundary layer transition on the MEXICO blade ECN-WIND-2018-006. MSc Thesis at the University of Applied Sciences Flensburg.
[8] White F M 1991 *Viscous Fluid Flow* (Mc. Graw Hill International Editions) ISBN: 0-07-100995-7 chapter 5 pp 335 - 90
[9] Van Ingen J L 2008 The e^N method for transition prediction. Historical review of work at TU Delft *38^{th} Fluid Dynamics Conference and Exhibit* AIAA 2008-3830
[10] Arnal D 1986 Diagrammes de stabilité des profils de couche limite auto-semblables en ecoulement bidimensionnel incompressible, sans et avec courant de Retour Technical Report OA Nr. 34/5018, ONERA
[11] Windte J, Radespiel R, Scholz U and Eisfeld Bernhard 2004 RANS simulation of the transitional flow around airfoils at low Reynolds numbers for steady and unsteady onset conditions RTO-MP-AVT-111
[12] Van Ingen J L 2006 The method of transition prediction. Historical review 1956-2006 of work at Delft aerospace low speed laboratory; Including a new version of the method, CD-ROM Edition, CD-ROM design and realization by J.Bongers.
[13] Montgomerie B et al. 1996 Three dimensional effects in stall ECN-C-96-079
[14] Parra E A 2016 Data reduction and analysis of New MEXICO experiment ECN-WIND-2015-189